Regularization of Bending and Crossing White Matter Fibers in MRI Q-Ball Fields

Hans-H. Ehricke [1] , Kay-M. Otto [1] and Uwe Klose [2]

[1] Institute for Applied Computer Science (IACS), Stralsund University

and

[2] MR Research Group, Dptm. of Diagnostic and Interventional Neuroradiology, University Hospital Tübingen

Corresponding author:
Prof. Dr. Hans-Heino Ehricke, Stralsund University, Institute for Applied Computer Science, Zur Schwedenschanze 15, D-18435 Stralsund, Germany, Fax: +49-3831-45711674, e-mail: hans.ehricke@fh-stralsund.de

Abstract

In diffusion MRI with high angular diffusion imaging (HARDI) a set of techniques has become available that allows better acquisition and representation of multi-directional diffusion profiles, e.g., in voxels with crossing, branching, and kissing fibers. The poor spatial resolution and low signal-to-noise ratio of the data, particularly when acquired under clinical conditions, prevent tractography algorithms from reliably reconstructing complex white matter structures. With cone-beam regularization (CB-REG) an inter-voxel smoothing approach has been described which in this paper is refined and adapted to fibers with subvoxel bending. By introducing the concept of asymmetric orientation distribution functions (aODFs) we are able to sharpen diffusion profiles of bending fibers and estimate subvoxel curvature. We also propose a deterministic fiber-tracking algorithm that exploits the enhanced resolution of asymmetric ODFs. The approach is evaluated quantitatively and compared with state-of-the-art noise-supression techniques in a study with a biological diffusion phantom. Moreover, we present results from an in-vivo study in which we demonstrate the method's ability to optimize tractography of bending fiber pathways of optic radiation.

Keywords: Diffusion MRI, Q-Ball Imaging (QBI), tractography, regularization, noise-supression, signal processing, optic radiation

1 Introduction

In diffusion magnetic resonance imaging (diffusion MRI), only a few methods have found their way into the clinical routine despite the continuous efforts of the scientific community. Diffusion tensor imaging (DTI) and deterministic streamline tracking are two such methods. In DTI the diffusion behavior of water molecules is described by a tensor with three eigenvectors and corresponding eigenvalues. Usually, the principal eigenvector is used as an estimate of a fiber's orientation. Streamline fiber-tracking approaches based on DTI have been proven to yield good results in the reconstruction of dominant fiber structures within brain white matter. The DTI method is less reliable for the delineation of more complex white matter structures, such as kissing, crossing, or branching fibers, which represent more than 30 percent of white matter tissue, as stated in [**?**]. In these situations, the single-tensor model with three orthogonal direction vectors is too simple to describe the diffusion behavior within a voxel. Due to the spatial resolution of diffusion MRI on the order of 2-3 mm, a voxel usually contains a

bunch of axons from one or more fiber bundles. Therefore, acquisition, reconstruction and post-processing techniques are needed that are capable of considering multiple fiber orientations within a voxel. By sampling a 3D grid, e.g., with diffusion spectrum imaging (DSI) [**?**], the probability density function of particle diffusion displacement may be reconstructed. However, long acquisition times prevent clinical application of this method. Another method is high angular resolution diffusion imaging (HARDI), which uses a huge number of evenly spaced gradient directions to sample a spherical shell. With q-ball imaging (QBI) a model-free reconstruction of an orientation distribution function (ODF) from the HARDI signal is performed [**?**]. Other reconstruction approaches are spherical deconvolution [**?**, **?**] and generalized DTI [**?**], both of which are model-dependent. Methods which may successfully be applied to diffusion data with relatively low angular resolution are super-resolved spherical deconvolution [**?**] and persistant angular structure MRI [**?**]. Another promising approach to the detection of multiple fiber directions is usage of multi-tensor models [**?**, **?**, **?**, **?**, **?**, **?**].

All methods mentioned above are basically capable of resolving multiple fiber orientations within a voxel, but the results very much depend on various factors, such as signal-to-noise ratio (SNR), fiber crossing angles and volume fractions of nondominant fibers. Most of the techniques share the drawbacks of time-consuming acquisition protocols and high susceptibility to artifacts (e.g., resulting from eddy currents or motion shift), and especially to noise. This is true also for QBI, on which we focus in this paper. In order to enhance the method's clinical practicality, noise suppression and direction field regularization techniques are needed that optimize the sharpness of the reconstructed diffusion profile prior to tracking. While intravoxel noise suppression schemes are state of the art in QBI, only a few approaches have been proposed for regional filtering taking into account the local voxel neighborhood [**?**] [**?**]. Cone-beam regularization (CB-REG) represents a straightforward yet effective method that allows sharpening of diffusion profiles by a filter scheme using samples from a local voxel neighborhood [**?**]. Initial results have demonstrated the method's ability to enhance tracking of nondominant fiber pathways through crossing regions. However, the CB-REG algorithm has the tendency to straighten fiber pathways and waits for a more accurate evaluation. In this paper, we address these problems by presenting algorithmic innovations together with quantitative and qualitative evaluation results.

2 Theory

As explained above, QBI is a model-independent reconstruction of the HARDI signal, leading to a diffusion orientation distribution function (ODF). The ODF reconstruction is performed by the application of a Funk-Radon transform (FRT) using either spherical radial basis functions (sRBF) [**?**] or spherical harmonics [**?**, **?**]. An ODF for a voxel at a discrete position (x_i, y_i, z_i) in 3D space may be imagined as a projection of diffusion probabilities p_{ij} onto the surface of a unit sphere constructed around that voxel. Each diffusion probability p_{ij} corresponds to a discrete reconstruction point r_j on the unit sphere surface, which can be defined by azimuthal/inclination angles (ϕ_j, υ_j). For each of the reconstructed surface points r_j, its ODF value p_{ij} describes the diffusion probability in direction $\overline{r_j}$ given by the unit vector from the sphere's center to the surface point. Thus, we can describe an ODF as a discrete functional:

$$\Psi_i(r_j) = p_{ij} \tag{1}$$

For reasons of symmetry, it is sufficient to distribute the data points r_j on a hemisphere: $\phi \in [0..2\pi], \upsilon \in [0..\pi]$. However, our regularization of the algorithm will lead to asymmetric ODFs (aODFs) with a distribution of data points on the full sphere.
If we use the probability value p_{ij} as a distance parameter describing the distance of the data point from the voxel center, we can transform the sphere model into a model of more complex shape, geometrically revealing the angular diffusion profile (Fig. 1a). In Fig. 1 color coding was used to illustrate diffusion directions (red: left-right, green: anteroposterior, blue: superior-inferior). The sharpness of this geometric representation is enhanced by normalization to the minimum-to-maximum signal interval, thus producing a min-max normalized ODF (Fig. 1b). However, the SNR of the ODF is typically quite low due to the restrictions of the imaging method. Therefore, an ODF may be smoothed locally by applying a spherical convolution matrix [**?**]. The kernel width defines the extent of a data point's neighborhood on the sphere, in which samples contribute to smoothing (Fig. 1c). Another approach of local smoothing is the application of the Laplace-Beltrami operator in the framework of a spherical harmonics approximation, thus reducing the influence of higher-order terms due to noise [**?**]. Especially in low-anisotropy regions of crossing and branching fibers, local smoothing is to be applied with great caution because it may suppress important details, e.g., signals originating from nondominant fibers.

Over the last five years, a variety of authors have proposed novel HARDI-

based approaches that pursue the idea of tracing pathways through areas of low diffusion anisotropy and thus allow tracking of non-dominant pathways through crossing regions. Many of these techniques focus on tracking algorithms. Both multiple-orientation deterministic methods and highly sophisticated and computationally more expensive probabilistic techniques [?, ?, ?, ?, ?] have been designed. It has been demonstrated that these novel techniques could improve results, when applied to the delineation of specific brain regions with more complex white matter populations. Nevertheless, we are far from having a general solution that would be clinically applicable.

3 Methods

3.1 Diffusion MRI Regularization

In image processing, regularization techniques are typically used in the framework of image enhancement. Their goal is to smooth the image intensity function by noise reduction, while preserving structural information. Various approaches to diffusion MRI have been introduced in the last decade, most of which focus on DTI regularization. They may be categorized by (1) smoothing of diffusion-weighted images prior to tensor reconstruction [?, ?], (2) incorporation of the regularization process into tensor estimation [?, ?], and (3) regularization of tensor fields [?, ?, ?].
Only a few of the approaches mentioned above may be transferred to HARDI-based imaging. It has been demonstrated that better fiber reconstruction results may be achieved by ODF smoothing within a voxel [?, ?]; these techniques are widely used today due to their computational effectiveness. However, by limiting the data source to signal values available within the voxel, the effect of the noise-suppression procedure is limited and the angular resolution of the data usually is reduced. A technique, commonly used in image processing, is to operate on a regional neighborhood, incorporating information from neighboring voxels into the process. Caution is advised when using these regional operators so as to avoid the suppression of structural information, such as the blurring of object edges. For this reason, more sophisticated noise-suppression approaches use structural information to steer the smoothing process. For example, with anisotropic diffusion filtering [?], the intensity gradient magnitude is used to scale the filter function, and thus smoothing over different objects is avoided. In order to impose the a priori knowledge of diffusion continuity across voxels, Savadjiev et al. [?] model fibers using chains of helical segments. They use the notion of co-helicity in

order to compute confidence values for ODF directions of neighboring voxels. Three neighboring directions are co-helical when the direction vectors may be regarded as tangents of a helix segment, thus yielding a high confidence value for that direction. Summing up the confidence values for a direction over the local neighborhood provides an estimate of local support. An iterative relaxation technique is used to maximize average local support. This method is highly sophisticated and showed good results when applied to the reconstruction of crossing fibers in phantom and in-vivo studies. Jonasson et al. [**?**] use ODF regularization prior to the segmentation of major white matter tracts. They transfer the ODF dataset to a five-dimensional non-Euclidian position orientation space. Within this space they use an anisotropic diffusion filter with an increasing number of iterations in order to produce multiple scales of resolution for the data. However, spatial resolution and ODF sharpness decrease with increasing degree of regularization. Therefore, it remains unclear whether the approach might successfully be used in white matter tractography. A completely different approach is to incorporate modeling assumptions into the reconstruction procedure. For example, a single-fiber response function may be used to deconvolve the diffusion-weighted signal or the diffusion ODF, thus producing a sharper fiber ODF [**?**, **?**].

3.2 A Generalized CB-REG Algorithm

In the case of ODF de-noising, our goal is to design a filter scheme that allows smoothing along fiber trajectories while preventing smoothing across fibers. When we reduce noise, the shape of the ODF becomes sharper and is more aligned with the underlying fiber architecture. Thus, the ODF field's consistency is enhanced. With CB-REG we have developed a method that avoids smoothing over anisotropic regions with different diffusion orientations by using structural information given by the ODF function itself [**?**]. Since the approach has not yet been presented to a broad audience, we will start with a short overview of the basic idea. We apply smoothing to each data point p_{ij} on the ODF sphere at position (x_i, y_i, z_i) in 3D space. The local neighborhood of the data point is defined by its direction vector $\overrightarrow{r_j}$ and two parameters α and l, describing the opening angle and length of the cone-shaped neighborhood, respectively, from which we draw samples for smoothing. The cone is centered on the direction vector $\overrightarrow{r_j}$ (cone A). Since the ODF is a symmetric function, a second cone B is constructed in the opposite direction $-\overrightarrow{r_j}$. Within each cone, rays are sent along all direction vectors $\overrightarrow{r_k}$ encompassed by the cone shape: $\angle(\overrightarrow{r_k}, \overrightarrow{r_j}) \leq \frac{\alpha}{2}$. Each ray is then sampled by interpolation of ODFs at each unit step along the ray until the base of the cone has been reached. Of all the ODFs sampled

along a certain ray, only the single data point whose direction coincides with the ray direction is relevant. All relevant data points p_{mk} that have been sampled inside the cone, are used for computing a smoothed ODF value $\tilde{\Psi}_i(r_j)$ by a weighted sum. We apply a two-dimensional Gaussian kernel $G(d, \delta)$ to scale each data point's weight according to its Euclidean distance $d_{mi} = \sqrt{(x_m - x_i)^2 + (y_m - y_i)^2 + (z_m - z_i)^2}$ from the voxel center and the angle $\delta_{kj} = \angle(\overrightarrow{r_k}, \overrightarrow{r_j})$ between its direction $\overrightarrow{r_k}$ and the direction $\overrightarrow{r_j}$ on which the cone is centered. Thus, the filtered ODF value $\tilde{\Psi}_i(r_j)$ is derived from the sampled ODF values $p_{mk} = \Psi_m(r_k)$ by

$$\tilde{\Psi}_i(r_j) = \frac{1}{w} \sum_{m \in M, k \in K} G(d_{mi}, \delta_{kj}) \Psi_m(r_k) \tag{2}$$

where
M: set of sampled positions within cone A and cone B
K: set of sampled ray directions within cone A and cone B
w: sum of all weights of the sampled data points within cone A and cone B:

$$w = \sum_{m \in M, k \in K} G(d_{mi}, \delta_{kj}) \tag{3}$$

and

$$G(d, \delta) = e^{-\frac{d^2}{\sigma_d^2} - \frac{\delta^2}{\sigma_\delta^2}}. \tag{4}$$

The parameters σ_d and σ_δ define the widths of the two-dimensional Gaussian function along and perpendicular to the cone's main axis. Thus, the two parameters define the sharpness of the Gaussian kernel, whereas the parameters α and l determine the size of the conic neighborhood region from which samples are drawn.
In our evaluation studies with this basic CB-REG algorithm we found that (1) the large number of filter parameters diminishes the practicality of the approach and (2) the discontinuity of cutting off weights at cone borders is a systematic problem. Therefore, we propose to generalize the algorithm by not restricting sampling to a conic neighborhood around a data point, thus extending the Gaussian kernel. In this manner, samples are drawn from wherever substantial weights ($G(d, \delta) > 0.01$) can be computed. The smoothing process is controlled solely by a two-dimensional Gaussian kernel, constructed around the data point's direction vector as well as around its opposite direction. Only two parameters, namely σ_d and σ_δ, have to be defined by the user. Figure 2 shows their influence on the shape of the resulting ODF in two examples: (1) Voxel from a rectangular crossing with a dominant and

a non-dominant fiber, derived from a phantom study. (2) Voxel from a crossing with an acute angle, derived from a proband dataset. The datasets from which the examples have been taken are described later in this paper. It is obvious that by increasing σ_d from 0.5 voxel to 3.5 voxel the contributions of neighbors along the data point's direction vector are increased, thus sharpening the ODF profile and allowing a second direction to be detected by a simple local maximum search. On the other hand, σ_δ controls the influence of neighboring directions, including data points from within the voxel. The larger its value, the higher is the influence of neighboring directions, which in the case of a crossing reduces noise, but also the sharpness of the diffusion profile.

3.3 Asymmetric CB-REG

Another extension of the CB-REG approach refers to the symmetry feature of the ODF function. For each direction $\overrightarrow{r_j}$ and opposite direction $-\overrightarrow{r_j}$, the ODF value is identical and therefore it is sufficient to store ODF values for a hemisphere. This is reasonable as long as we regard only data points within a voxel. Since opposite directions define two neighborhoods containing different voxels representing different anatomic regions, it seems straightforward to distinguish between them, when calculating $\tilde{\Psi}_i(r_j)$. This can be done by increasing the weights of the samples from neighborhood A while decreasing them for neighborhood B. Thus, we get different ODF values for $\overrightarrow{r_j}$ and $-\overrightarrow{r_j}$, and the resulting ODF is no longer symmetric. This approach leads to an improved measure of the local orientations. The data points r_j are distributed on a full sphere: $\phi \in [0..2\pi], \upsilon \in [0..2\pi]$.

To implement this asymmetric CB-REG method, it is sufficient to specify different parameters σ_d and σ_δ for sample weighting from opposite directions. In order to increase the influence of the neighborhood in direction $\overrightarrow{r_j}$, we may define a higher value for σ_{d,r_j} than for $\sigma_{d,-r_j}$. Alternatively, the parameters σ_{δ,r_j} and $\sigma_{\delta,-r_j}$ may be defined in an analogous manner. The resolution-enhancing effect of this strategy allows a better representation of diffusion profiles in regions with bending fibers. Figure 3 illustrates the sampling scheme used in asymmetric cone-beam regularization applied to a single data point (violet arrow). The relevant data points (red arrows) from the ODF samples (green) are weighted by gaussian kernels, symbolized by the cloud-like background. In dark regions high weights are used, whereas a light background color means a low weighting factor.

3.4 A Deterministic Algorithm for Tracking Asymmetric ODFs

Fiber pathways were tracked by means of a deterministic approach, based on the method by Perrin et al. [**?**]. They propose a particle-tracing technique in which a particle entering a voxel with a certain speed and motion direction is deflected by a force originating from the local q-ball. The orientation of the force is chosen randomly inside a cone, defined from the incident direction. The ODF data points within the cone are used to control the random process. The main drawback of this approach is that the reconstructed fibers systematically diverge with increasing distance from the seed region. We have adapted this method to deterministic fiber tracking by substituting the random selection process. In our approach, the trajectory direction is derived from the incident direction and the ODF of the sample. When tracking with symmetric ODFs, we define a cone centered on the incident direction. Only those data points on the sphere encompassed by the cone are taken into account. We select the tracking direction by determining the ODF's maximum within the cone. We stop tracking if the cone's maximum is less than 60 percent of the ODF's overall maximum, because then we can no longer assume anisotropic behavior with sufficient safety and might generate unrealistic connections. Otherwise, the direction vector of the maximum value is used for the next step of the integration process along the fiber pathway. A further stopping criterion is the sample's generalized fractional anisotropy (minimum: 0.2). This tracking method is similar to the deterministic ODF tracking algorithms described in [**?**, **?**], but does not support tracking of branching fiber pathways.

Due to the improved measure of local orientations in aODFs, it is useful to consider data points on the sphere not only around the incident direction, but also on the opposite side. To implement an asymmetric tracking algorithm we use a twofold decision strategy with two conic regions. As explained in Fig. 4, first we construct a cone around the opposite $-r_{in}$ of the incident direction vector. If the ODF maximum within this cone satisfies the above mentioned tracking criteria, the sample is accepted as a continuation of the fiber. In this case, the maximum's direction r_{max1} is flipped by 180°. A second cone is constructed around $-r_{max1}$. If the ODF maximum within this cone satisfies the tracking criteria, we proceed tracking in the maximum's direction r_{max2}. The cone's opening angles define the maximum deviation ϕ_{max} of the incident tracking direction. We use a stricter criterion for the acceptance of the sample under investigation by reducing the opening angle of cone 1 and applying a relationship of $1 : 1.5$ to opening angles of cones 1

and 2.

3.5 Data Acquisition

Diffusion phantom data provided by McGill University, Montreal, was used for the quantitative evaluation of the regularization approach described in this paper. The phantom was constructed from excised rat spinal cord, embedded in agar in a configuration designed to have curved, straight, and crossing tracts [**?**] (Fig. 5). The q-ball data were acquired on a 1.5 Tesla Sonata MR scanner (Siemens, Erlangen) with 90 diffusion-weighting directions, 30 slices, a b-value of 1300 s/mm^2 and an isotropic resolution of 2.8 mm. We are aware of the fact that the phantom's crossing area is not totally realistic, because there is partial voluming, but no real intersection of the two cords. Nevertheless, we prefer usage of a biological phantom, because in terms of diffusion signal behavior we are nearer to an in-vivo situation, than with synthetic phantoms, such as those decribed in [**?**, **?**]. Moreover, the focus of this paper is on bending fiber pathways, which in the McGill phantom data is represented by two highly realistic curvature regions with non-constant curve angles.
We also applied our method to data from healthy volunteers acquired with a spin-echo EPI sequence on a 3 Tesla Trio scanner (Siemens, Erlangen) with an isotropic resolution of 2.0 mm, 64 gradient directions, and 56 slices ($TR = 8\ s, TE = 105\ ms, b = 2000$ s/mm $^2, 108 * 108\ matrix$). In order to arrive at clinically tolerable acquisition times of maximum 10 minutes, we did not use multiple acquisitions with averaging.

ODFs were reconstructed on the basis of the spherical harmonics approach. We project the ODF onto the sphere tesselated with a mesh, giving 100 sample directions on the hemisphere. Due to computer memory restrictions we did not use finer tesselations.

4 Results

4.1 Phantom Study

Figure 5 presents the generalized fractional anisotropy (GFA) values from a slice through the phantom dataset (a). The original ODFs, reconstructed with spherical harmonics ($l = 4$), are illustrated by the zoomed ODF shape display of the crossing region (b). The lower row displays results of ODF regularizations with different parameters. Since in the crossing area fiber

pathways possess an almost linear geometry, symmetric CB-REG was used in this case. The results illustrate that regularization sharpens the ODFs, with the effect becoming more obvious as parameter σ_d increases. The regularized ODFs within the fiber-crossing area clearly show the expected bidirectional anisotropic behavior.

We also applied the symmetric tracking algorithm described above to phantom data, which were sharpened by the application of different intravoxel and regional regularization schemes:

1. Numerical ODF reconstruction using a Funk-Radon transform (FRT) and angular smoothing with a 15° spherical Gaussian kernel [**?**].
2. ODF reconstruction based on spherical harmonics and smoothing with Laplace-Beltrami (LB) operator ($l = 8, \lambda = 0.006$) as proposed in [**?**].
3. ODF reconstruction with spherical harmonics ($l = 8$) and CB-REG with (a) $\sigma_d = 2.5$ voxel, $\sigma_\delta = 20°$ and (b) $\sigma_d = 3.0$ voxel, $\sigma_\delta = 10°$.
4. Laplace-Beltrami smoothing as in point (2.) above and CB-REG with $\sigma_d = 2.5$ voxel, $\sigma_\delta = 0°$ (without angular smoothing).

Figure 6 shows the streamlines that were generated by using two rectangular seed regions (red/yellow boxes in Fig. 5), demonstrating the qualitative differences between the three regularization approaches. The tracking algorithm was parameterized with a maximum deviation angle ϕ_{max} of 30°. Application of the CB-REG method allows a greater number of the fibers of the two crossing spinal cords to be reconstructed. Table 1 presents a quantitative analysis, giving the number of fibers in the straight (red) and the curved (yellow) cords that can be traced through the crossing region, originating from 240 and 245 seeds. The figures show that CB-REG may successfully be used for intravoxel as well as for regional noise-smoothing and ODF sharpening (configurations 3a and 3b). Furthermore, the combination of CB-REG without intravoxel smoothing ($\sigma_\delta = 0°$) in the Laplace-Beltrami approach yields good results, as may be derived from comparing configurations 3a and 4.

A second study analyzed the high-curvature segment of the phantom data. Here, we tried to track the bending fibers without prior application of the CB-REG algorithm. Instead, a Laplace-Beltrami regularization with $\lambda = 0.006$ was performed. As shown in Fig. 7, it was possible to reconstruct the bending cord only in part. A slightly better result was achieved by using the

	# fibers (straight)	# fibers (curved)
(1) FRT + Gaussian kernel (15°)	13/240	24/245
(2) SH + LB ($l = 8, \lambda = 0.006$)	33/240	41/245
(3a) SH + CB-REG ($\sigma_d = 2.5$ v., $\sigma_\delta = 20°$)	77/240	73/245
(3b) SH + CB-REG ($\sigma_d = 3.0$ v., $\sigma_\delta = 10°$)	95/240	91/245
(4) SH + LB (2) + CB-REG ($\sigma_d = 2.5$ v., $\sigma_\delta = 0°$)	98/240	75/245

Table 1: Comparison of noise-supression methods (FRT = Funk-Radon transform, SH = spherical harmonics, LB = Laplace-Beltrami operator).

asymmetric CB-REG approach with $\sigma_{\delta,r_j} = 35°$, $\sigma_{\delta,-r_j} = 10°$ and $\sigma_d = 1.5$ voxel, together with symmetric tracking. Only in cases where the asymmetric tracking strategy was applied to ODFs that were smoothed by asymmetric CB-REG could nearly the entire cord be delineated. All tracking results were achieved with a maximum deviation angle ϕ_{max} of 35°.

4.2 In-Vivo Data

In our in-vivo study we focused on the delineation of fiber pathways of the optic tract, radiating out of the lateral geniculate nucleus (LGN) to the visual cortex. This optic radiation consists of three large fiber bundles, the central and dorsal bundles and the anterior ventral bundle also termed Meyer's loop. Meyer's loop runs anteriorly around the tip of the inferior horn, passes posteriorly along the lateral wall of the ventricle, and converges on the lower lip of the calcarine fissure (Fig. 8). Along its course it passes through regions of crossing and kissing fibers and reveals sections of strong bending, thus making it a good candidate for the evaluation of the asymmetric CB-REG approach. Due to a high intersubject variability it is essential to determine its exact anatomy prior to temporal lobe neurosurgery in order to prevent damage to the visual fiber system [**?**, **?**]. We placed rectangular seed regions in the LGNs and a huge target ROI in a dorsal location (Fig. 9). In a first experiment, tracking was performed without prior CB-REG application. ODFs were reconstructed on the basis of the spherical harmonics approach with order $l = 6$ and Laplace-Beltrami regularization with $\lambda = 0.006$. The best result could be achieved by parameterization of the tracking algorithm with a maximum deviation angle ϕ_{max} of 35°. However, Meyer's loop could be reconstructed on one side only. On the other hand, both loops could be delineated when applying our asymmetric CB-REG approach together with the asymmetric tracking strategy. We used $\sigma_{\delta,r_j} = 35°$, $\sigma_{\delta,-r_j} = 10°$, and $\sigma_d = 2.0\, voxel$ for CB-REG and were able to reduce the maximum deviation

angle ϕ_{max} to 18°. This experiment shows that the reconstruction of high-curvature fiber pathways, such as Meyer's loop, from noisy data measured under clinical conditions may be optimized by the application of asymmetric CB-REG.

4.3 CB-REG Parameter Selection

A signal processing method's practicality not only depends on its robustness, but also on the number and sensitivity of the parameters which have to be selected by the user. Since the regional processing scheme of the CB-REG approach is not limited to the data within a voxel, such as in most signal reconstruction or intra-voxel smoothing methods, the task of parameter selection depends not only on diffusion signal features, e.g., SNR. Rather, geometry and architecture of fiber pathways which are to be reconstructed, have to be regarded. While the sampling step width may standardly be set to 0.25 voxels, the parameters σ_d and σ_δ of the two-dimensional gaussian are more critical. Due to the complex dependency on signal and geometry features, an automatic parameter selection mechanism is hard to find. From our experiments with the phantom dataset as well as various in-vivo studies with acquisition protocols employing 64 or 126 gradient encoding directions and b-values between 1000 and 2000 s/mm^2 we found the following procedure and settings to be helpful. If we want to track non-dominant fiber pathways through crossing areas, σ_d may be derived from the area's size. If the crossing ranges over i voxels, setting σ_d to $i-1$ is a good choice. This allows the width of the gaussian kernel to be determined such that samples from voxels which represent fiber continuation outside the crossing, are included. An example for a wide-area crossing situation is given by transcallosal fibers radiating out to the cerebral cortex as non-dominant pathways through regions of crossing projective and associative fiber bundles, e.g., the fronto-occipital fascilus. Here, we achieved good results with $\sigma_d = 3.0$ on a dataset with a spatial resolution of 2 mm. The parameter σ_δ is set according to the signal's SNR. For a SNR in the range of 30 to 40, which we usually can expect from a high-quality acquisition, a value of 15° may be used. For lower-quality data the value may be increased up to 20°. If the goal is to reconstruct high-curvature pathways with fiber orientations which differ by more than 35° between neighboring voxels, the application of asymmetric CB-REG with $\sigma_{\delta,r_j} = 35°$ and $\sigma_{\delta,-r_j} = 10°$ reliably yields good results. In this case σ_d may be set to a voxel range which covers approx. 4 mm. Although these recommendations are a first step to the practical application of the method, we currently work on a more thorough analysis of parameter

optimization on the basis of simulation data for different fiber architectures.

5 Discussion and Conclusions

We have presented a generalization of an algorithmically straightforward yet effective method for the regularization of q-ball fields. We use a directionally weighted spatial averaging scheme to enhance the representation of non-dominant fibers in the ODF profile and reduce noise. The method may be parameterized to produce asymmetric ODFs that better represent high-curvature sections of fiber pathways. Tractography with aODFs is enhanced by means of a deterministic algorithm considering data points on both sides of the q-ball: around the incoming and the opposite direction. Our experiments show that tracking fiber pathways through crossing regions and bending structures benefits from the regularization of the q-ball field. The method is useful particularly when applied to noisy data, which typically are the result of measurements under clinical conditions. Our preliminary results from experiments with datasets, acquired with more time-consuming protocols, e.g., with 126 gradient directions and multiple acquisitions with signal averaging, show that the positive effect of intervoxel smoothing decreases with growing SNR, as expected. Since the method includes both (1) noise-supression with samples from within a voxel and (2) regularization with a voxel neighborhood, it possesses a high degree of generality. In comparison to methods which regularize diffusion tensor fields by bringing diffusion tensors in good agreement with surrounding tensors [**?**, **?**, **?**], we here focus on a model-free reconstruction of the diffusion profile and thus have to regard all possible diffusion directions. We would like to point out that the method is computationally expensive. Regularization of a whole dataset may take up to an hour on a standard desktop central processing unit (CPU). However, the process may be easily parallelized, thus exploiting multi-core architectures and graphical processing units (GPUs), available on standard desktop computers. Moreover, it is not usually necessary to regularize the dataset as a whole, but rather the CB-REG module may be integrated into the fiber-tracking process such that only the ODFs that are needed during tracking are regularized. Thus, we can reduce the amount of CB-REG processing time to a range of several seconds to minutes, depending on track lengths and the number of seeds.

Despite the method's robustness, the question of parameter optimization needs further study. Although we currently perform a detailed analysis with simulated datsets, we are aware of the fact, that the outcome of simulation studies may not easily be transfered to in-vivo data. However, we expect

that we can come up with more specific recommendations than those given in the previous chapter. Another open issue for further investigation is usage of different HARDI reconstruction techniques, e.g., spherical deconvolution or multi-tensor approaches, prior to regularization with CB-REG. Can the asymmetric inter-voxel regularization concept achieve similar results, if fiberODFs are used as input? We would like to point out that the idea of taking into account samples from a regional neighborhood may also be applied in tractography algorithms in order to better estimate the most probable direction for the next integration step. It has been demonstrated that this can help to solve ambiguities that are still existent in ODFs in which noise has been reduced by local smoothing operators [**?**, **?**]. So, these tractography approaches may be regarded as an alternative to or an extension of the methodology proposed in this paper.

Acknowledgments

We would like to thank Jennifer Campbell of the McConnell Brain Imaging Centre, Montreal Neurological Institute, McGill University, for providing the phantom data we used in our experiments. We also would like to thank Vinod Kumar of the University Hospital Tübingen, Section of Magnetic Resonance in the CNS, for making the in-vivo data available.

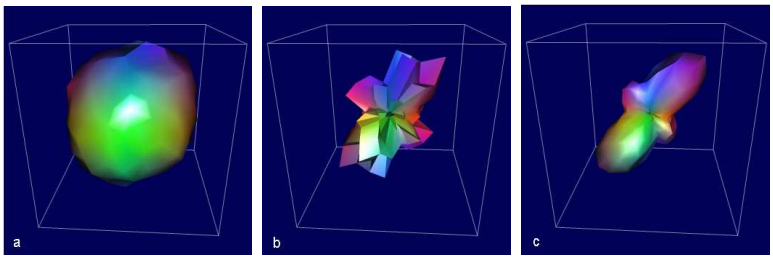

Figure 1: Reconstruction of diffusion profile in a voxel by ODF. From left to right: (a) Directionally color-encoded ODF surface, in which the distance of a surface point from the center represents diffusion probability, (b) min-max normalized ODF, (c) min-max normalized and locally smoothed ODF.

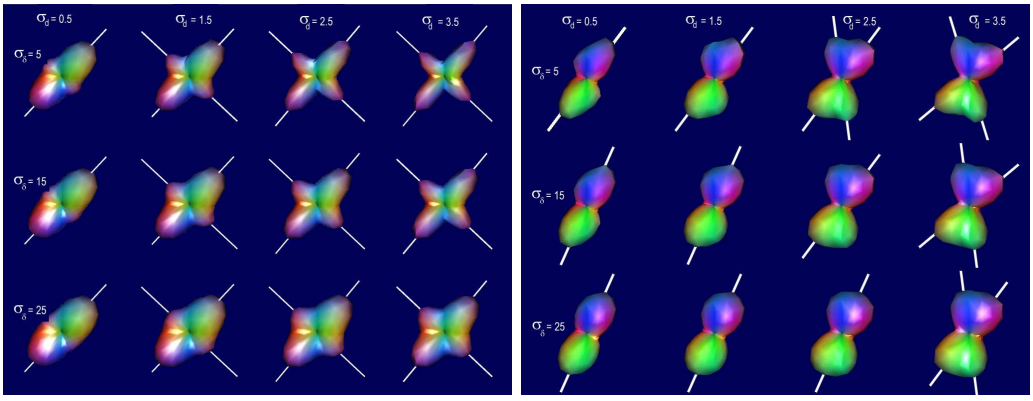

Figure 2: Influence of parameters σ_d and σ_δ on ODF shape. Left: Rectangular crossing with a non-dominant fiber. Right: Crossing with an acute angle.

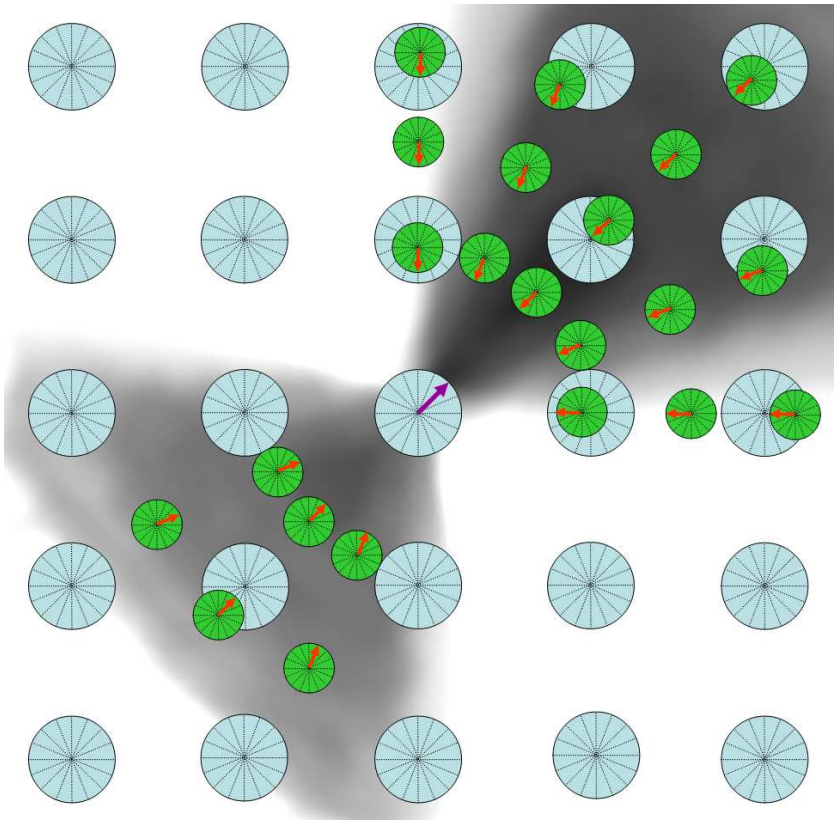

Figure 3: Sketch of neighborhood sampling strategy used in asymmetric cone-beam regularization for a single ODF data point (violet arrow): Original ODFs (blue) and interpolated samples (green) with relevant data points (red arrows). The cloud-like background illustrates the weighting factors of the gaussian kernels.

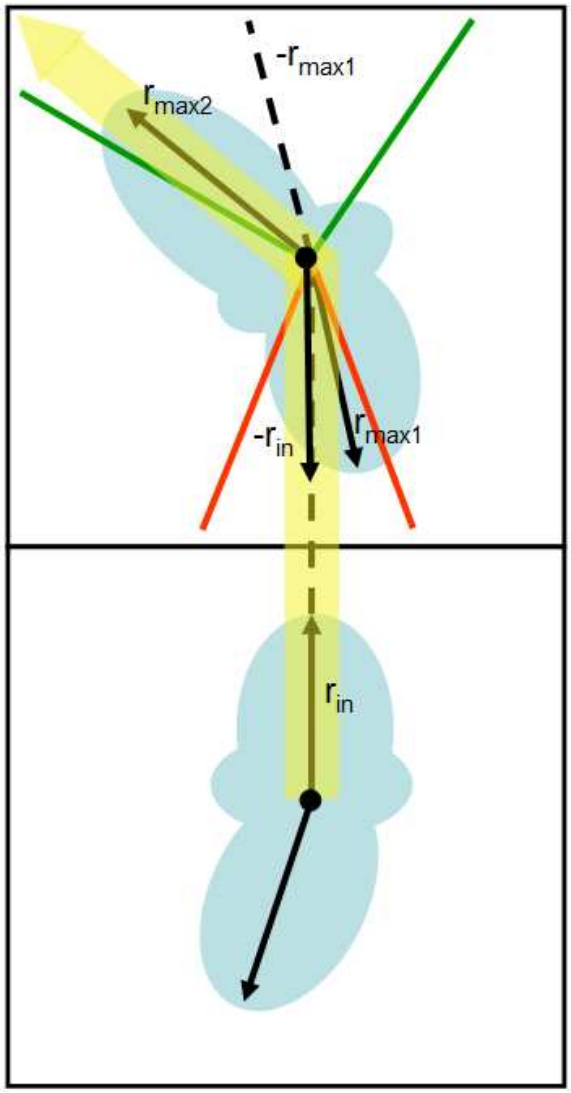

Figure 4: Extrapolating tracking direction (yellow) with aODFs (blue) using data points from two conic regions: Cone 1 (red) constructed around opposite $-r_{in}$ to incident direction and cone 2 (green) around opposite $-r_{max1}$ to ODF maximum within cone 1.

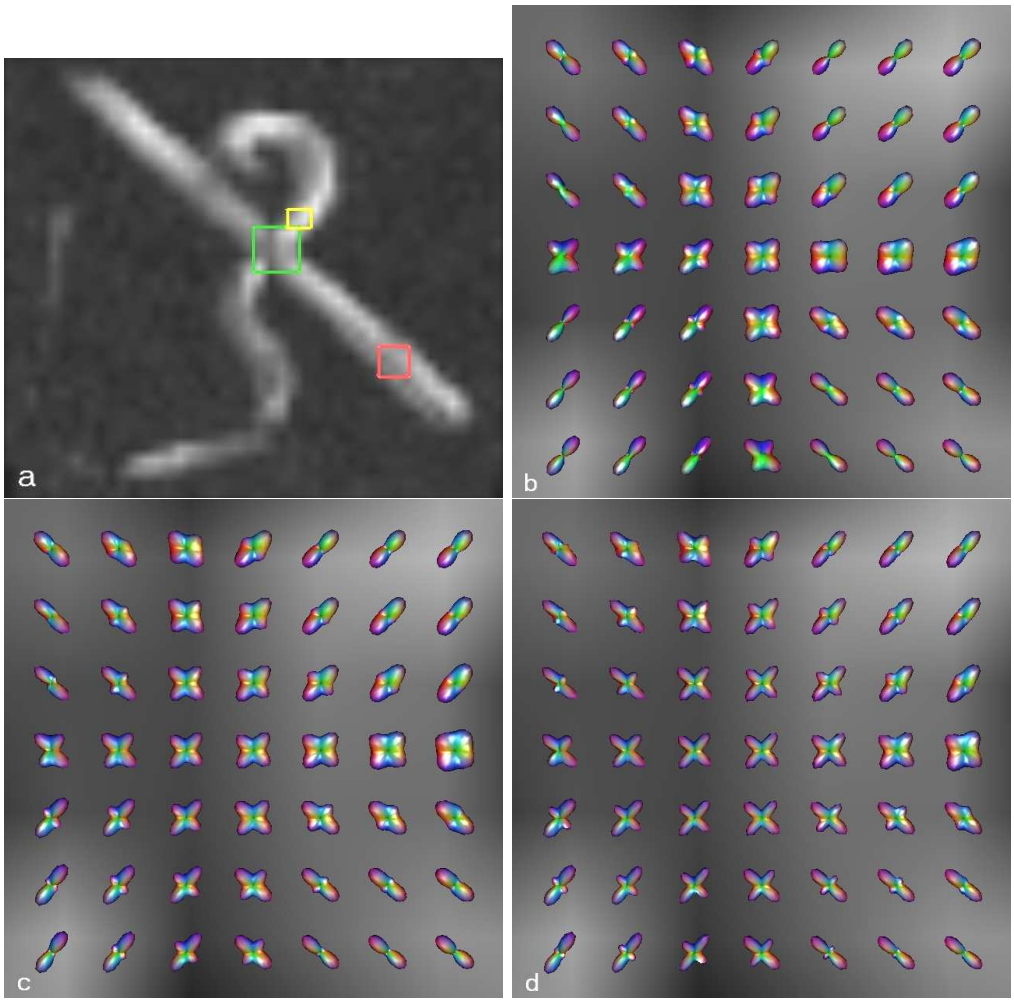

Figure 5: Regularization impact on ODF shape in a crossing area of the phantom: (a) phantom shape (GFA values) with region of interest (green) and seed regions (red, yellow), (b) original ODFs in region of interest, (c) ODFs in region of interest after application of CB-REG with $\sigma_d = 2.5$ voxel and $\sigma_\delta = 20$, (d) ODFs in region of interest after application of CB-REG with $\sigma_d = 3.0$ voxel and $\sigma_\delta = 10$.

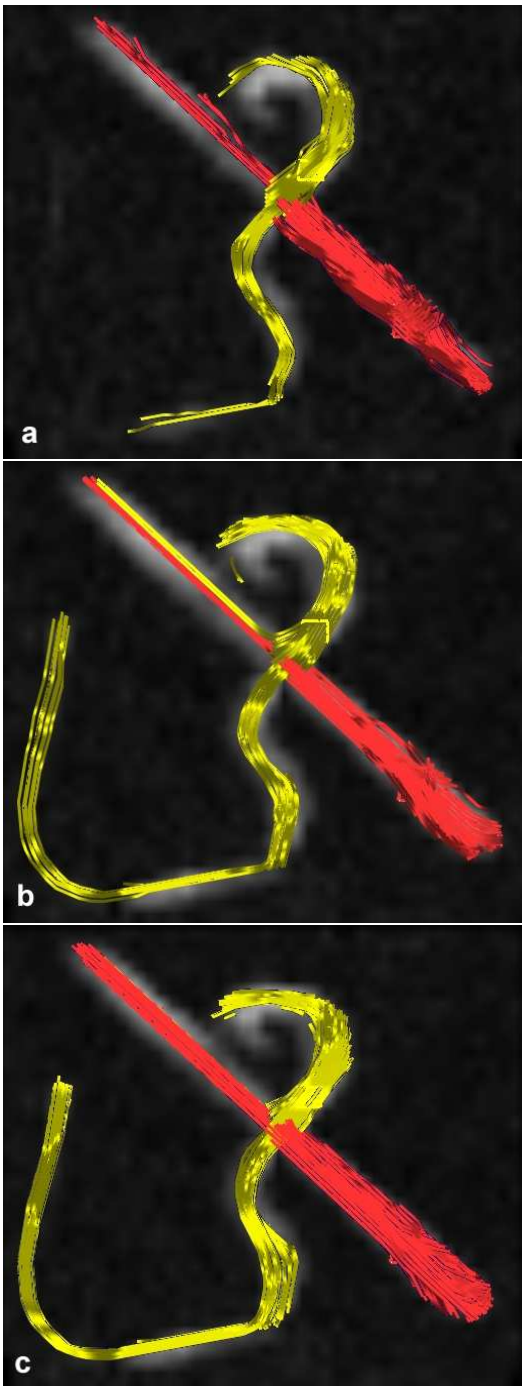

Figure 6: Tracking result from phantom study with ODFs from different regularization methods: (a) FRT and Gaussian kernel ($\sigma = 15°$), (b) spherical harmonics approximation ($l = 8$) + Laplace-Beltrami operator ($\lambda = 0.006$), and (c) CB-REG with $\sigma_d = 3.0\,voxel$ and $\sigma_\delta = 10$.

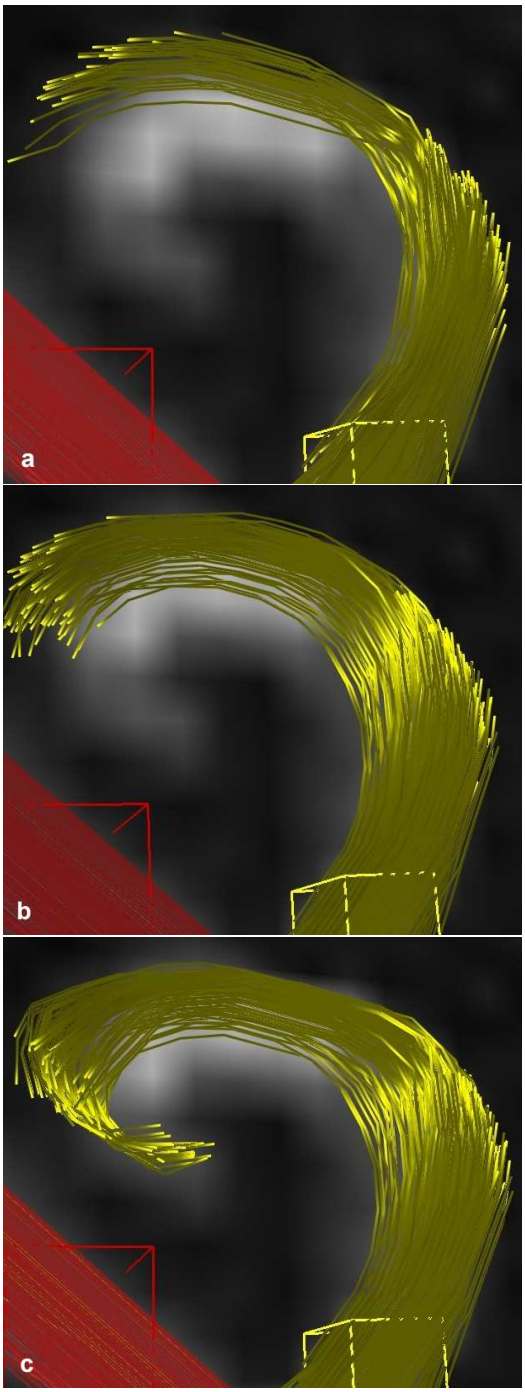

Figure 7: Tracking results of a high-curvature pathway from the phantom study: (a) without CB-REG, (b) with asymmetric CB-REG and symmetric tracking algorithm, (c) with asymmetric CB-REG and asymmetric tracking.

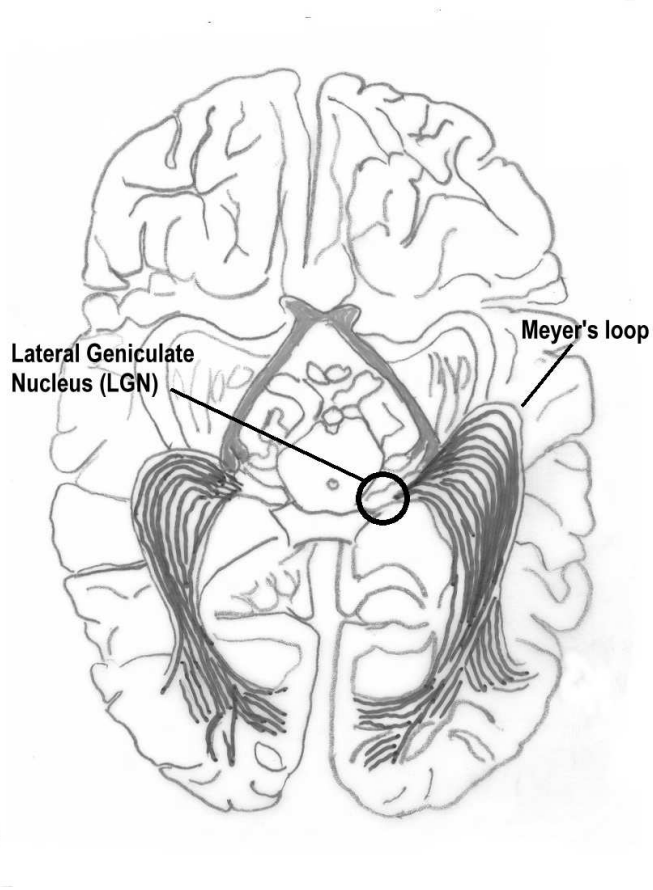

Figure 8: Anatomic sketch of optical tract with Meyer's loop and LGN, viewed from below.

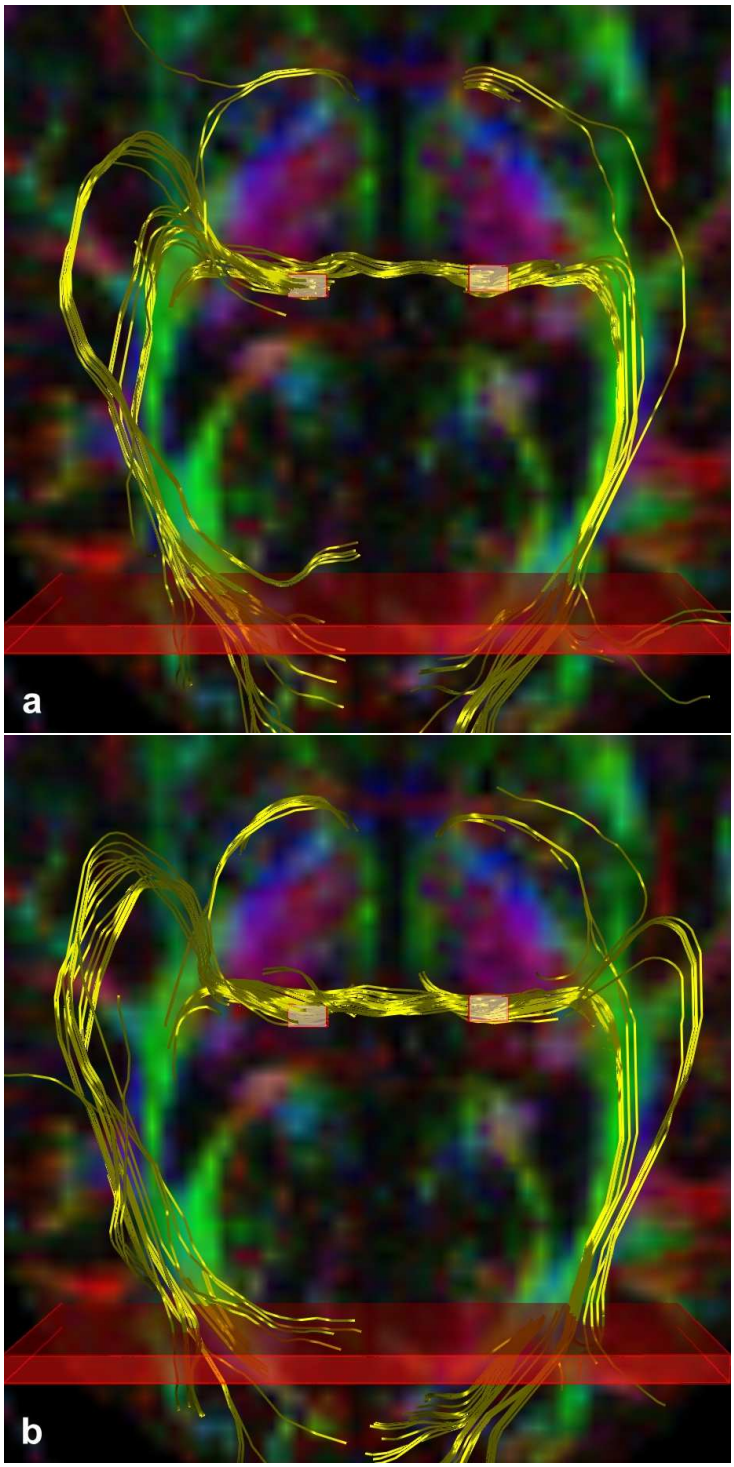

Figure 9: Seed boxes, target ROI, and tracking results for Meyer's loop (a) before and (b) after asymmetric regularization.